TISSUE ENGINEERING: Part C
Volume 21, Number 7, 2015

DOI: 10.1089/ten.tec.2014.0527

Noninvasive Quantitative Imaging of Collagen Microstructure in Three-Dimensional Hydrogels Using High-Frequency Ultrasound

Karla P. Mercado, MS,[1] María Helguera, PhD,[2] Denise C. Hocking, PhD,[3,*] and Diane Dalecki, PhD[1,*]

Collagen I is widely used as a natural component of biomaterials for both tissue engineering and regenerative medicine applications. The physical and biological properties of fibrillar collagens are strongly tied to variations in collagen fiber microstructure. The goal of this study was to develop the use of high-frequency quantitative ultrasound to assess collagen microstructure within three-dimensional (3D) hydrogels noninvasively and nondestructively. The integrated backscatter coefficient (IBC) was employed as a quantitative ultrasound parameter to detect, image, and quantify spatial variations in collagen fiber density and diameter. Collagen fiber microstructure was varied by fabricating hydrogels with different collagen concentrations or polymerization temperatures. IBC values were computed from measurements of the backscattered radio-frequency ultrasound signals collected using a single-element transducer (38-MHz center frequency, 13–47 MHz bandwidth). The IBC increased linearly with increasing collagen concentration and decreasing polymerization temperature. Parametric 3D images of the IBC were generated to visualize and quantify regional variations in collagen microstructure throughout the volume of hydrogels fabricated in standard tissue culture plates. IBC parametric images of corresponding cell-embedded collagen gels showed cell accumulation within regions having elevated collagen IBC values. The capability of this ultrasound technique to noninvasively detect and quantify spatial differences in collagen microstructure offers a valuable tool to monitor the structural properties of collagen scaffolds during fabrication, to detect functional differences in collagen microstructure, and to guide fundamental research on the interactions of cells and collagen matrices.

Introduction

Collagen-based biomaterials are widely investigated as scaffolds for tissue engineering and regenerative medicine applications. The microstructure of collagen hydrogels can be tuned for specific applications by altering fabrication parameters, including bulk collagen concentration,[1] temperature,[2,3] pH,[4,5] ionic strength,[4] culture media type,[6] gel thickness,[5,6] pepsin treatment,[5,7] or exposure to mechanical forces during collagen self-assembly *in vitro*.[8] The structural properties of collagen scaffolds can influence cell behaviors key to tissue regeneration, including cell migration, differentiation, and proliferation.[1,6,9] Therefore, the development of quantitative technologies capable of visualizing spatial differences in collagen fiber microstructure under various fabrication conditions will provide critical tools to facilitate the development of functional engineered tissue constructs.

Techniques currently used to evaluate collagen fiber density or structure have distinct limitations that restrict their utility in tissue engineering applications. Histological analysis requires time-consuming and destructive processing procedures, evaluates only small sections of the sample, and does not provide information about collagen fibril structure. Microscopy-based techniques, such as second harmonic generation (SHG) microscopy, confocal reflectance microscopy (CRM), and scanning electron microscopy (SEM), have been employed to evaluate key structural characteristics of collagen fibrils, including density, thickness, and alignment.[1–7,10] However, SHG and CRM have penetration depths of less than 1 mm and narrow focal widths, limiting the ability to image large volumes of thick hydrogels. SEM is destructive and requires sampling of a small fraction of the tissue under investigation. Further, SHG, SEM, and CRM are expensive technologies, often with limited availability. In this investigation, we develop a novel ultrasound

[1]Department of Biomedical Engineering, University of Rochester, Rochester, New York.
[2]Chester F. Carlson Center for Imaging Science, Rochester Institute of Technology, Rochester, New York.
[3]Department of Pharmacology and Physiology, University of Rochester, Rochester, New York.
*Senior co-authors.

technology to overcome these limitations by enabling nondestructive, quantitative, real-time, volumetric imaging of three-dimensional (3D) collagen scaffolds. Ultrasound is well suited for tissue engineering applications as it is cost effective, portable, and can be integrated into tissue fabrication environments.

Conventional B-scan ultrasound imaging has been widely used as a clinical diagnostic tool to qualitatively visualize the structure of native tissues. B-scan ultrasound has also been used to monitor extracellular matrix synthesis in 3D fibrin gels embedded with myofibroblasts,[11] evaluate changes in extracellular matrix deposition during chondrogenic differentiation of adipose stem cells in 3D poly(lactide-co-glycolide) scaffolds,[12] estimate cell density in β-tricalcium phosphate scaffolds embedded with bone marrow stromal cells,[13] and evaluate the phase inversion process of drug-releasing, poly(lactic-co-glycolic acid) implants.[14] B-scan ultrasound imaging utilizes the envelope of the backscattered radio-frequency (RF) echoes to generate a gray-scale image of tissue structure. B-scan images are highly dependent upon system settings and, therefore, provide only qualitative images of structure. Importantly, B-scan ultrasound cannot provide quantitative, system-independent metrics to characterize tissue properties because it is affected by imaging system parameters, such as the frequency response of the ultrasound system, the receiver gain, and other operator settings.[15–17]

Ultrasound tissue characterization techniques have been developed to overcome the limitations of B-scan imaging, and enable quantitative assessments of tissue properties of both normal and diseased tissues.[17] Quantitative ultrasound techniques have employed various parameters to characterize tissues, including the speed of sound,[18,19] absorption and attenuation coefficients,[18,20] nonlinearity parameter,[21] angular scattering,[22] backscatter coefficient,[23–25] integrated backscatter coefficient (IBC),[18,25,26] effective scatterer diameter,[27] midband fit,[16,28,29] spectral intercept,[28] and spectral slope.[16,28,29] These parameters can provide estimates of the density, size, and spatial organization of acoustic scatterers in tissue.[23,24] Unlike B-scan imaging, quantitative ultrasound approaches are independent of the ultrasound system and operator settings, and can provide metrics for tissue characterization. Quantitative ultrasound techniques currently under investigation have been applied to a broad range of native tissues.[17] As examples, quantitative ultrasound techniques have been used to characterize various tumors,[19,30] evaluate cardiac abnormalities,[31] monitor cell death,[29,32] characterize human dermis and subcutaneous fat,[33] and assess therapeutic responses in diseased tissues.[27,34,35]

Several recent studies have shown that quantitative ultrasound can provide an important tool for the field of tissue engineering.[36] The midband fit and spectral slope parameters were employed to evaluate the mineral content of collagen constructs with hydroxyapatite[16] and monitor osteoblastic differentiation in engineered tissues *in vitro*.[37] Ultrasound elasticity imaging has been investigated for monitoring the elastic properties of polyurethane-based scaffolds subcutaneously implanted in mice and in a rat abdominal repair model.[38,39] We previously demonstrated the utility of the IBC as a metric for quantifying cell concentration noninvasively within 3D cell-embedded agarose hydrogels, where the ultrasound was backscattered predominantly from cells.[25]

In this study, a high-frequency quantitative ultrasound technique was developed to nondestructively and noninvasively characterize the microstructure of 3D acellular collagen scaffolds. We hypothesized that the IBC can be employed as a metric to quantitatively detect differences in collagen fiber microstructure, namely fiber density and diameter, throughout the volume of 3D acellular hydrogels. The absence of cells in the collagen hydrogels enabled assessment of collagen fiber microstructure using high-frequency ultrasound. Parametric images of the IBC were generated to quantitatively visualize regional variations in collagen fiber microstructure volumetrically. IBC imaging of collagen gels embedded with fibroblasts was then utilized to visualize and quantify the response of cells to regional variations in collagen microstructure within 3D hydrogels.

Materials and Methods

Fabrication of collagen hydrogels

Neutralized type I collagen solutions were prepared on ice by combining type I collagen (BD Biosciences; from rat tail tendon) with 2× phosphate-buffered saline (PBS) and 1× PBS such that the final mixture contained 1× PBS and collagen at concentrations of 1, 2, or 4 mg/mL. Both 1× and 2× PBS were degassed in a vacuum chamber for 30 min before incorporation into the collagen mixture. Collagen mixtures (4 mL) were placed in cylindrical Teflon sample holders that were 16 mm thick and 20 mm in diameter. The open circular faces of the tubular holders were sealed with Saran™ Wrap (S.C. Johnson & Son, Inc.). The Saran membranes separated the collagen gel from the external environment, and provided an acoustic propagation path with reduced reflections. For experiments that varied the bulk collagen concentration, collagen mixtures at concentrations of 1, 2, or 4 mg/mL were incubated at 37°C for 1 h. Five separate gels were investigated for each collagen concentration. For experiments that varied the polymerization temperature, 2 mg/mL collagen samples were allowed to polymerize for 1 h at either 22°C or 37°C. Five separate gels were investigated for each polymerization temperature.

In other experiments, acellular and cell-embedded collagen gels were fabricated in 12-well tissue culture plates (Corning, Inc.). Acellular gels were fabricated by combining type I collagen with 2× Dulbecco's modified Eagle's medium (DMEM; Invitrogen) and 1× DMEM such that the final mixture contained 1× DMEM and collagen at a concentration of 2 mg/mL. The 1× and 2× DMEM were degassed in a vacuum chamber for 30 min before incorporation in the collagen mixture. The collagen mixture was then incubated at 37°C, 8% CO_2 for 1 h to allow for collagen polymerization. Each acellular gel was 22 mm in diameter. The thickness of acellular gels was 2, 4, or 9 mm. At least three separate acellular gels were analyzed for each gel thickness. Mouse embryonic fibroblasts were cultured as described previously.[25] Cell-embedded, 2 mg/mL collagen gels were fabricated by mixing fibroblasts with collagen and 1× DMEM to obtain a final cell concentration of 4×10^5 cells/mL. Gels were then incubated at 37°C, 8% CO_2 for 1 h. Each cell-embedded gel was 22 mm in diameter and 9 mm thick. Three separate cell-embedded gels were analyzed.

TABLE 1. MEASURED TRANSDUCER CHARACTERISTICS

Transducer characteristics	*Model PI50-2*
Center frequency	38 MHz
Aperture diameter	6.35 mm
Focal distance	21 mm
F-number	3.3
Beam width (−6 dB)	170 μm
Pulse length (−6 dB)	41 μm
Depth of field (−6 dB)	4.7 mm
Bandwidth (−6 dB)	13–47 MHz

Transducer characterization

Experiments were performed using a single-element, polyvinylidene fluoride (PVDF) focused ultrasound transducer (PI50-2; Olympus). An 85-μm diameter PVDF hydrophone (HGL-0085; Onda Corp.) was used to measure the acoustic beam pattern of the transducer. The −6 dB beam width and depth of field were computed from the measured beam patterns. The power spectrum of the RF echo from a planar steel reflector was used to determine the frequency response of the ultrasound system (i.e., reference spectrum)[25,40] and the −6 dB bandwidth of the transducer. Table 1 provides the characteristics of the ultrasound transducer.

Acoustic attenuation measurements

Acoustic attenuation coefficients of collagen gels and intervening Saran membranes were determined using a through-transmission, narrowband, insertion-loss technique, using water at 21°C as the reference medium.[41,42] Attenuation measurements were obtained within the −6 dB bandwidth of the transducer in 1-MHz steps using a hydrophone (HGL-0085; Onda Corp.). Samples were polymerized for 1 h before performing attenuation measurements. The average attenuation coefficient of the collagen with intervening Saran membranes was calculated using measurements from four separate samples for each collagen concentration and each polymerization temperature. The attenuation coefficients were used to compensate for the frequency and depth-dependent acoustic attenuation through the collagen gels and intervening Saran membranes, as described previously.[25]

Backscatter data acquisition

Experimental setups used to measure ultrasound backscatter from collagen gels are shown in Figure 1. Figure 1A illustrates the setup used to collect backscattered RF signals from collagen hydrogels in Teflon holders. The gel holder and ultrasound transducer were placed in a plastic tank containing degassed, deionized water at a room temperature of 21°C. The transducer was mounted on a 3-axis positioner (Velmex, Inc.), controlled by a custom Matlab® program (Mathworks, Inc.). The transducer was aligned such that the focal region was at an axial location of 2 mm into the collagen gel.

The setup used to measure backscattered signals from collagen gels in tissue culture plates is depicted in Figure 1B. The wells of tissue culture plates that contained gels were filled with 1× DMEM with 25 mM HEPES before performing backscatter measurements. An acoustic standoff containing degassed, deionized water was placed above the well to provide an acoustic propagation path. A Saran membrane at the bottom of the standoff separated water from DMEM. Tissue culture plates were positioned at the top of the water tank to reduce the amplitude of reflections from the bottom of the plate. Acoustic reverberations from the interfaces between the water, collagen gel, Saran membrane, and bottom of the plate were not present in the imaging field of view. The transducer focus was positioned at various axial depths within the gels, in depth increments of 1 mm, to collect backscatter measurements throughout the entire thickness of the gel.

In both experimental setups, a pulser/receiver (5073PR; Olympus) was used to generate a broadband pulse that excited the transducer at a pulse repetition frequency of 1 kHz. Ultrasound backscattered signals were amplified and digitized to 12 bits using a digital oscilloscope (Waverunner 62Xi-A; LeCroy Corp.) at a sampling frequency of 500 MHz. Signal-to-noise ratio was improved by averaging 60 repeated

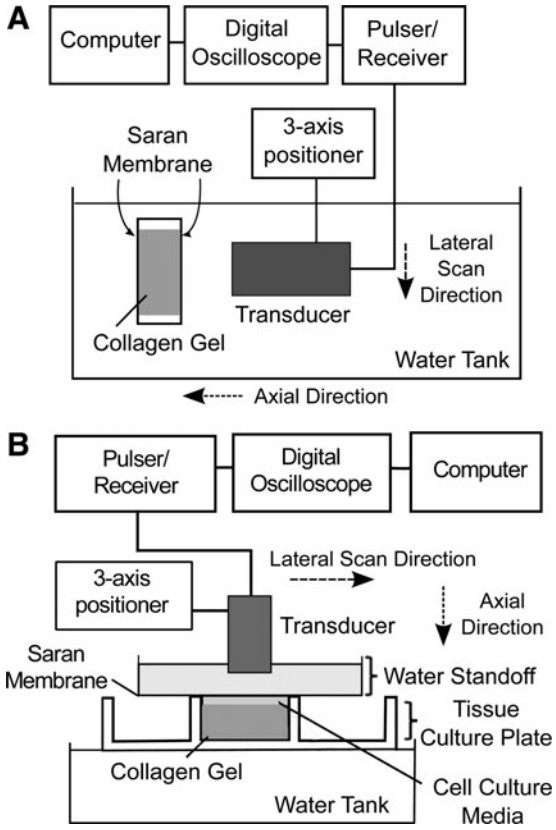

FIG. 1. Schematics of experimental setups. **(A)** Collagen gels (16 mm thick, 20 mm in diameter) were fabricated in cylindrical Teflon sample holders sealed with Saran™ membranes. The sample and the transducer were placed in a water tank with degassed, deionized water. **(B)** Acellular collagen gels (2, 4, or 9 mm thick) and gels with cells (9-mm thick gel with 4×10^5 cells/mL) were fabricated in 12-well tissue culture plates. After collagen polymerization was complete, wells were filled with cell culture media, and a water standoff was placed above the well to provide a path for acoustic propagation. The tissue culture plate was positioned at the top of a water tank to reduce reflections from the bottom of the plate. In both setups, a single-element transducer was aligned using a 3-axis positioner such that its focus was within the collagen gel. A pulse/receiver supplied radio-frequency (RF) signals that excited the transducer, and received the backscattered RF signals from the gel.

RF acquisitions at each scan location.[20,25] The transducer was laterally translated to scan an imaging plane. Neighboring RF lines in each imaging plane were separated by 106 μm (greater than half of a beam width) and were independent of each other.[43] Backscattered RF measurements from collagen gels in Teflon holders were conducted at five independent imaging planes in each gel. Forty-eight RF lines (spanning a 5-mm lateral distance) were collected per imaging plane. Raster scans of the collagen gels fabricated in tissue culture plates were conducted in 106-μm steps in the lateral and transaxial (x, y) directions. Each raster scan contained 189 independent imaging planes, each consisting of 189 independent RF lines. The raster scan volume was 15 mm axially, and 20 mm laterally and transaxially. The ultrasound transducer was positioned such that the collagen gel was at the center of the raster scan volume.

IBC estimation

In experiments that investigated collagen gels fabricated in Teflon holders, five independent imaging planes were scanned in each collagen gel. Five collagen gels were investigated for each collagen concentration and polymerization temperature. A B-scan image was generated offline for each imaging plane by calculating the grayscale envelope of each RF line and stacking the RF lines in the lateral direction. For each imaging plane, the B-scan image was used to select a region of interest (ROI) that contained 48 adjacent RF lines (Fig. 2A). Each ROI had a 1-mm axial length and was centered at the transducer's focal region. RF lines were scaled to compensate for the receive gain. A Hanning weighting function was applied to each RF line in the axial direction to reduce spectral side lobes (Fig. 2A). The IBC of the entire ROI was calculated using a custom Matlab program, as described previously.[25]

Microscopy

Immediately after performing ultrasound backscatter measurements, the Saran membrane on one side of the Teflon holder was removed. Collagen gels were fixed for 1 h using 4% paraformaldehyde and then washed 3× with PBS. SHG microscopy was conducted using an Olympus Fluoview 1000 AOM-MPM microscope, equipped with a 25×, 1.05 NA water immersion lens (Olympus), as described previously.[44] Images were collected in the z-direction in 5-μm steps at depths of 450–550 μm below the gel surface. Images were then projected onto the z-plane using ImageJ software (NIH).

Imaging regional variations in collagen microstructure

B-scan images of acellular collagen gels fabricated in tissue culture plates were generated as described above.

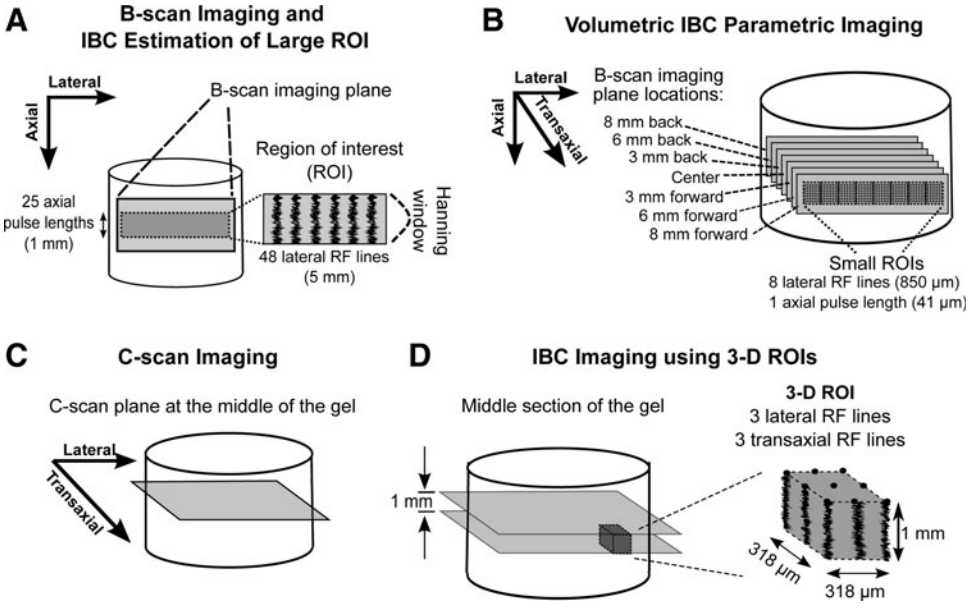

FIG. 2. Schematics of analyses of backscatter RF signals. **(A)** B-scan imaging and integrated backscatter coefficient (IBC) estimation of acellular collagen gels fabricated in Teflon sample holders. The transducer focus was positioned at an axial depth of 2 mm in the gel. Five independent B-scan imaging planes were scanned for each gel. A region of interest (ROI) was selected for each imaging plane and was comprised of 48 independent RF lines (5 mm lateral length) that were 1 mm axially (i.e., 25 pulse lengths long). The IBC was then calculated for each ROI. **(B)** Schematic demonstrating volumetric IBC imaging of acellular collagen gels fabricated in a tissue culture plate. Seven, independent B-scan imaging planes were obtained corresponding to regions located at the center, and 3, 6, and 8 mm in either direction from the gel center. Each scan encompassed the entire lateral distance of the gel. The transducer focus was positioned at various depths in the gel. In each imaging plane, multiple ROIs were selected to increase spatial resolution. Each ROI had dimensions of one axial pulse length (41 μm long) and eight RF lines (850 μm laterally). The IBC was calculated for each ROI, and a parametric image of the IBC was generated for each imaging plane. **(C)** Schematic of a C-scan imaging plane at the middle of a collagen gel fabricated in a tissue culture plate. **(D)** The middle section of the gel in the tissue culture plate was selected and divided into multiple 3D ROIs, each comprised of nine RF lines (three RF lines laterally, three RF lines transaxially) with an axial depth of 1 mm. The IBC was calculated for each ROI, and a parametric image was generated as a 2D IBC map in the lateral-transaxial plane.

Imaging planes were located at the gel center, and at 3, 6, and 8 mm from the gel center (Fig. 2B). Parametric images of calculated IBC values were created for each imaging plane[25] using backscattered RF data collected at various depths below the gel surface. IBCs were calculated for small ROIs, overlapped by 50% in the axial direction.[25,26] Each ROI had dimensions of eight RF lines (850 μm laterally) and one axial pulse length (41 μm).[43]

C-scan images of the same gels were generated by mapping the grayscale image of the ultrasound backscatter at the middle of the gel in a plane perpendicular to the direction of sound propagation (Fig. 2C). Subsequently, the backscattered data corresponding to the middle section of the gel (Fig. 2D) were used to generate a parametric image of IBC values.[25] Each ROI in the IBC image included 3D backscattered data, comprised of nine RF lines (three RF lines laterally, three RF lines transaxially) with an axial length of 1 mm (Fig. 2D).[25] The lateral and transaxial dimensions of each ROI were both 318 μm. Parametric images were then displayed as a map of IBC values in the lateral-transaxial plane. C-scan and IBC images of cell-embedded collagen gels fabricated in tissue culture plates were also generated and compared to those of acellular gels.

Statistical analyses

Means and standard deviations of attenuation coefficient measurements of collagen hydrogels fabricated with different collagen concentrations and at different polymerization temperatures were calculated. Power law regression analyses of attenuation measurements as a function of ultrasound frequency were performed. IBC estimates of collagen hydrogels are presented as mean ± standard error of the mean as a function of collagen concentration or polymerization temperature. Linear regression analyses of IBC estimates as a function of collagen concentration were performed. The coefficient of variation (CV) of IBC estimates was computed to investigate the precision of the IBC technique for each fabrication condition. Statistical comparisons were performed using either one-way analysis of variance or Student's *t*-test for unpaired samples, as appropriate. Results were considered statistically significant when $p < 0.05$. All statistical tests were performed using Matlab.

Results

Attenuation coefficient measurements of collagen gels

The frequency-dependent attenuation coefficients of collagen hydrogels with intervening Saran membrane were measured using the through-transmission, narrowband, insertion-loss technique for various fabrication collagen concentrations (Fig. 3A) and polymerization temperatures (Fig. 3B). The power law fits to the attenuation measurements for gels polymerized at 37°C, with collagen concentrations of 1, 2, and 4 mg/mL were $\alpha = 0.012f^{1.6}$, $\alpha = 0.016f^{1.6}$, and $\alpha = 0.024f^{1.5}$, respectively, where α is the attenuation coefficient (dB/cm) and f is the ultrasound frequency (MHz). The power law fits to the data corresponding to the 2 mg/mL collagen polymerized at 22°C and 37°C were $\alpha = 0.017f^{1.6}$ and $\alpha = 0.015f^{1.6}$, respectively. The power law equations were incorporated into the computation of the IBC to compensate for frequency and depth-dependent attenuation through the hydrogels and intervening Saran membrane, as described previously.[25]

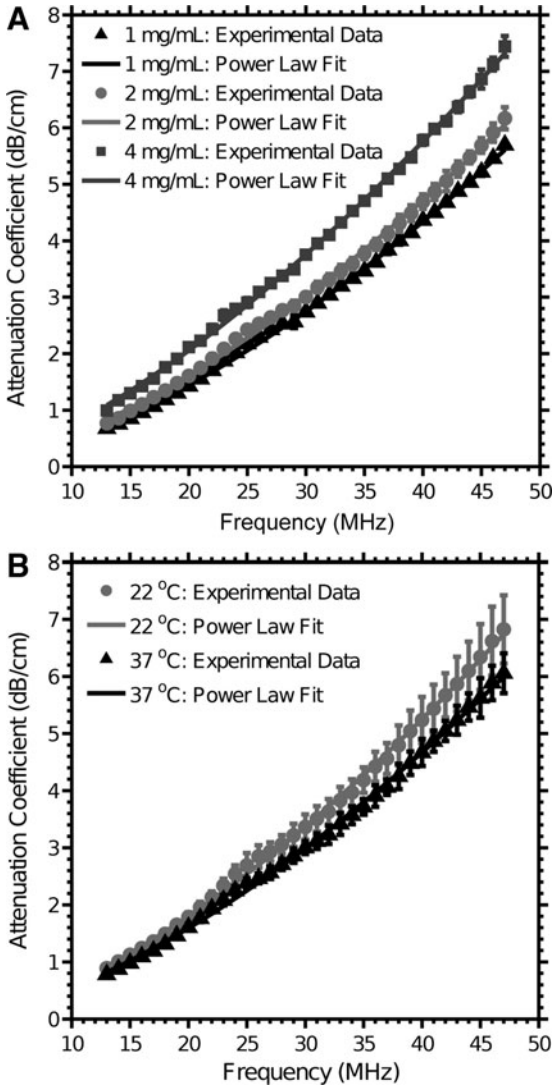

FIG. 3. Acoustic attenuation coefficients of collagen hydrogels. The insertion-loss technique was used to measure attenuation coefficients of collagen gels in Teflon sample holders (with intervening Saran membrane) fabricated with **(A)** 1 mg/mL (*black triangles*), 2 mg/mL (*light gray circles*), or 4 mg/mL collagen (*dark gray squares*) polymerized at 37°C, and **(B)** 2 mg/mL collagen polymerized at 22°C (*gray circles*) or 37°C (*black triangles*). Mean ± standard deviation of measured attenuation coefficients are shown ($n = 4$ collagen gels per fabrication condition). The *solid lines* represent power law fits to the measured data. The power law fit equations of the attenuation data for 1, 2, and 4 mg/mL collagen are $\alpha = 0.012f^{1.6}$, $\alpha = 0.016f^{1.6}$, and $\alpha = 0.024f^{1.5}$, respectively, where α is the attenuation coefficient (dB/cm) and f is the ultrasound frequency (MHz). The power law fits to the data corresponding to the 2 mg/mL collagen polymerized at 22°C and 37°C are $\alpha = 0.017f^{1.6}$ and $\alpha = 0.015f^{1.6}$, respectively.

B-scan imaging of collagen hydrogels with varied fiber microstructures

Collagen gels were polymerized using either different collagen concentrations or temperatures to produce known variations in collagen fiber density and diameter.[2,10] SHG microscopy images of the collagen gels confirmed the

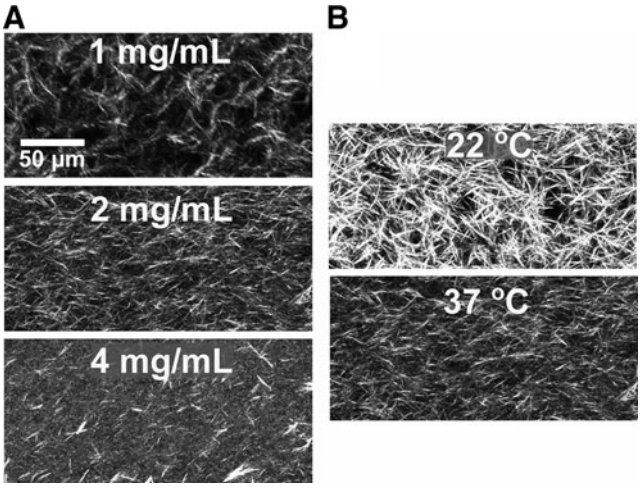

FIG. 4. Second harmonic generation microscopy images of collagen fibers in hydrogels. Collagen gels were fabricated in Teflon holders using **(A)** 1, 2, or 4 mg/mL collagen polymerized at 37°C, or **(B)** 2 mg/mL collagen polymerized at 22°C or 37°C. Imaging was performed at the center of the gel, and images were collected in the z-direction in 5-μm steps at depths from 450 to 550 μm below the gel surface. Images were then projected onto the z-plane using ImageJ software. Scale bar, 50 μm.

expected changes in collagen fiber microstructure in response to various fabrication conditions (Fig. 4). As demonstrated previously,[2,10] collagen fiber density increased as collagen concentration was increased from 1 to 4 mg/mL at a polymerization temperature of 37°C (Fig. 4A). Collagen fiber diameter in 2 mg/mL collagen gels was greater in gels polymerized at 22°C compared with gels polymerized at 37°C (Fig. 4B).

Representative B-scan images of collagen gels are shown in Figure 5. The echogenicity of the B-scan images of collagen gels increased as the collagen concentration was increased (Fig. 5A) and as the polymerization temperature was decreased (Fig. 5B). However, B-scan images provide only qualitative visualization of the microstructure of collagen gels.

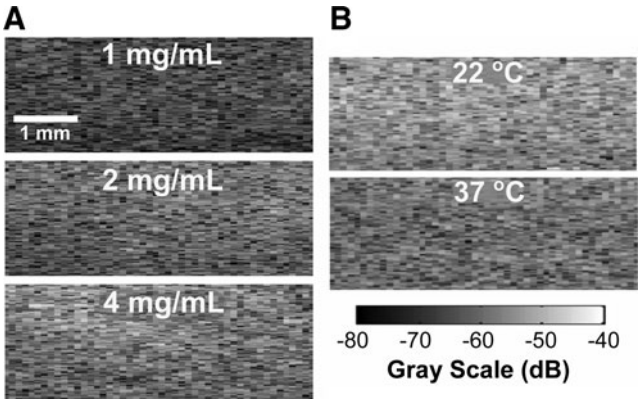

FIG. 5. B-scan images of collagen hydrogels. Shown are representative B-scan images of collagen gels that were fabricated in Teflon holders with **(A)** 1, 2, or 4 mg/mL collagen polymerized at 37°C, or **(B)** 2 mg/mL collagen polymerized at 22°C or 37°C. B-scan imaging was performed at five independent imaging planes in each gel ($n = 5$ samples per fabrication condition). The transducer was focused at an axial depth of 2 mm. Scale bar, 1 mm.

Measurements of IBCs of collagen hydrogels

IBC values for collagen gels fabricated in Teflon holders were computed from the measured backscattered data in selected ROIs[25] (Fig. 6). The mean ± standard error of the mean IBC was $0.3 \pm 0.03 \times 10^{-5}$ sr^{-1} cm^{-1}, $0.8 \pm 0.07 \times 10^{-5}$ sr^{-1} cm^{-1}, and $1.6 \pm 0.2 \times 10^{-5}$ sr^{-1} cm^{-1} for collagen gels with concentrations of 1, 2, and 4 mg/mL, respectively (Fig. 6A).

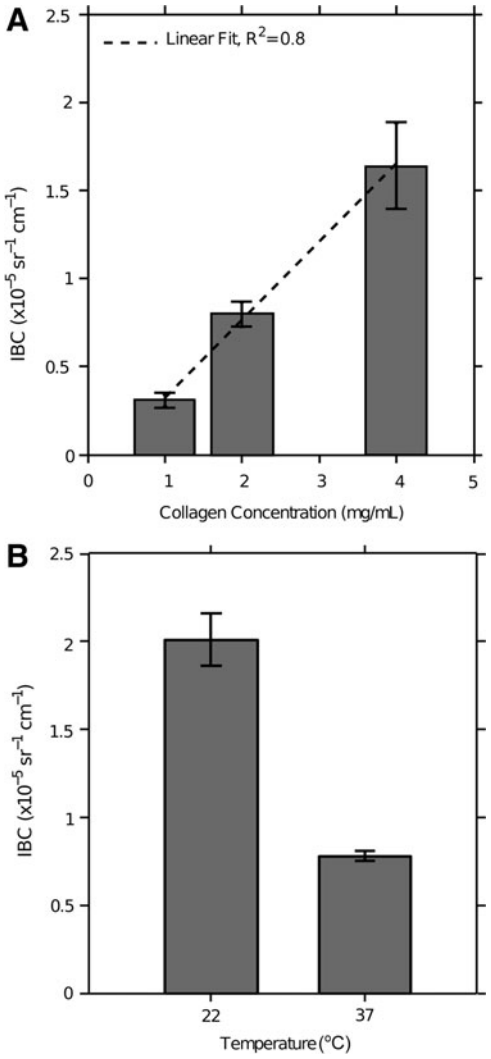

FIG. 6. IBC as a function of collagen concentration and polymerization temperature. Collagen gels were fabricated in Teflon sample holders using **(A)** 1, 2, or 4 mg/mL collagen polymerized at 37°C, or **(B)** 2 mg/mL collagen polymerized at 22°C or 37°C. The transducer was focused at an axial depth of 2 mm in the gel. The IBC was estimated using the backscatter RF data of selected ROIs in B-scan images. Each ROI had an axial length of 1 mm (i.e., 25 pulse lengths long) and a lateral length of 5 mm with 48 RF lines. Mean ± standard error of the mean of the IBC are shown ($n = 5$ samples per fabrication condition). A linear fit to the IBC estimates as a function of collagen concentration and corresponding regression coefficient R^2 are shown.

The IBC linearly increased with increasing collagen concentration (Fig. 6A), and these differences in IBC estimates among collagen concentrations were statistically significant ($p = 0.001$). The increase in IBC with collagen concentration was consistent with the increase in echogenicity observed in B-scan images (Fig. 5A), and with the increase in collagen fiber density observed in SHG images (Fig. 4A). Thus, increasing collagen fiber density enhanced ultrasound backscatter due to an increase in scatterer number density.[23]

The mean ± standard error of the mean IBC was $2.0 \pm 0.2 \times 10^{-5}$ sr^{-1} cm^{-1} and $0.8 \pm 0.03 \times 10^{-5}$ sr^{-1} cm^{-1} for 2 mg/mL collagen gels polymerized at either 22 or 37°C, respectively (Fig. 6B). The differences in IBC estimates between polymerization temperatures were statistically significant ($p < 0.001$). The decrease in IBC with increasing polymerization temperature is consistent with the decrease in echogenicity observed in B-scan images (Fig. 5B), and the decrease in collagen fiber size observed from SHG images (Fig. 4B). Thus, larger collagen fibers backscatter ultrasound more efficiently due to an increase in the acoustic scatterer size.[23]

The precision of the IBC technique was assessed by analyzing the CV of IBC estimates for each fabrication condition. The CVs of IBC estimates for collagen gels with concentrations of 1, 2, and 4 mg/mL were 5.7%, 4.6%, and 6.9%, respectively. The CVs of IBC estimates for 2 mg/mL collagen gels polymerized at either 22°C or 37°C were 3.9% and 4.0%, respectively. The acceptable level of precision for biochemical assays under development is typically less than 20% CV.[45] Taken together, these results demonstrate that high-frequency ultrasound based on the IBC can detect and precisely quantify changes in collagen fiber density and diameter in 3D hydrogels.

Volumetric imaging of collagen gels fabricated in tissue culture plates

Thus far, collagen hydrogels fabricated in the relatively large Teflon holders showed homogeneous collagen fiber microstructure throughout the volume of the gel (Figs. 4–6). Experiments were next conducted to evaluate collagen microstructure throughout the volume of gels polymerized in standard tissue culture plates. B-scan images of a representative acellular, 2 mg/mL collagen gel (9 mm thick), fabricated in a 12-well tissue culture plate, are shown for imaging planes through the gel center, and at 3, 6, and 8 mm from the gel center (Fig. 7A). B-scan images are arranged to provide a qualitative visualization of the regional variations in collagen microstructure over an axial depth from 3 to 6 mm below the gel surface. At this depth, a ring of collagen with enhanced echogenicity was observed at ~3 mm from the gel edge.

Parametric IBC images were next generated to quantify these regional variations in collagen microstructure (Fig. 7B). Color-scale IBC images were overlaid onto corresponding B-scan images to provide quantitative visualization of the regional variations in collagen microstructure within the gel (Fig. 7B). Each color pixel represents an ROI with eight RF lines (850 μm laterally) and an axial length of 41 μm (one pulse length). Quantitative IBC values within the echogenic ring were approximately five times greater than IBC values obtained at the center of the gel. The acquisition and arrangement of imaging planes in succession from the back to the front of the gel demonstrates the capability for volumetric IBC imaging of 3D collagen gels.

A C-scan image (Fig. 8A) of a plane in the middle of a similarly fabricated gel clearly shows this ring of increased collagen echogenicity. A quantitative IBC image at this C-scan plane is shown in Figure 8B. Each pixel in this IBC image corresponds to a 3D ROI (as illustrated in Fig. 2D) comprised of nine RF lines (three RF lines laterally, three RF lines transaxially) with 1-mm axial length. The IBC image provides a quantitative visualization of the higher collagen backscatter in a continuous 15-mm diameter ring located ~3 mm from the gel periphery (Fig. 8B).

To examine the significance of this ring of elevated collagen backscatter, fibroblasts were co-polymerized with 2 mg/mL collagen gels in 12-well plates at 37°C for 1 h. Representative C-scan (Fig. 8C) and corresponding IBC (Fig. 8D) images obtained through the middle (i.e., depth of 4.5 mm) of a cell-embedded collagen gel are shown. The C-scan image of the cell-embedded gel (Fig. 8C) was more echogenic than that of the acellular gel (Fig. 8A), and the backscatter pattern from the cell-embedded gel appeared qualitatively homogeneous (Fig. 8C). In contrast, the quantitative IBC image of the cell-embedded gel (Fig. 8D) revealed a ring of increased IBC values that was not evident in the qualitative C-scan image (Fig. 8C). Importantly, the colorbar scale of the IBC image of the cell-embedded collagen gel (Fig. 8D) is an order of magnitude greater than that of the acellular gel (Fig. 8B) because the cells are the dominant scatterers in the cell-embedded collagen gels.[25] Thus, a comparison of Figure 8B and D indicates that cells had accumulated within a region coincident with the ring of increased IBC observed within acellular collagen gels.

Additional studies demonstrated that regional variations in collagen fiber microstructure were also dependent on the thickness of collagen gels fabricated in 12-well tissue culture plates. B-scan images of acellular, 2 mg/mL collagen gels with thickness of either 2, 4, or 9 mm are shown for imaging planes at the gel center, and at 6 and 8 mm from the gel center (Fig. 9). B-scan images and corresponding quantitative IBC images showed distinct regional patterns of collagen backscatter that varied among the gels of different thickness (Fig. 9). B-scan and IBC images of 2-mm thick gels indicated homogenous collagen microstructure throughout the gel (Fig. 9A). In comparison, B-scan and IBC images of 4-mm thick gels showed regional variations in collagen microstructure, where the periphery and bottom regions had IBC values that were more than five times that of the central region of the gel (Fig. 9B). The B-scan and IBC images of 9-mm thick gels showed elevated IBC values at both the top and bottom of the gels, with a narrow (~1-mm wide) region of elevated collagen backscatter, ~3 mm from the gel edge extending vertically from the top to the bottom of the gel (Figs. 9C and 10). These data confirm that the ring of elevated IBC identified in the C-scan image through the center of the gels (Fig. 8) was present throughout the vertical height of the gels. Moreover, parametric IBC images of cell-embedded, 9-mm thick collagen gels revealed an inhomogeneous distribution of cells throughout the full thickness of the gels. The highest cell densities were observed at the periphery and bottom of the gels while the lowest cell densities were found within the central core of the gels (Fig. 10B).

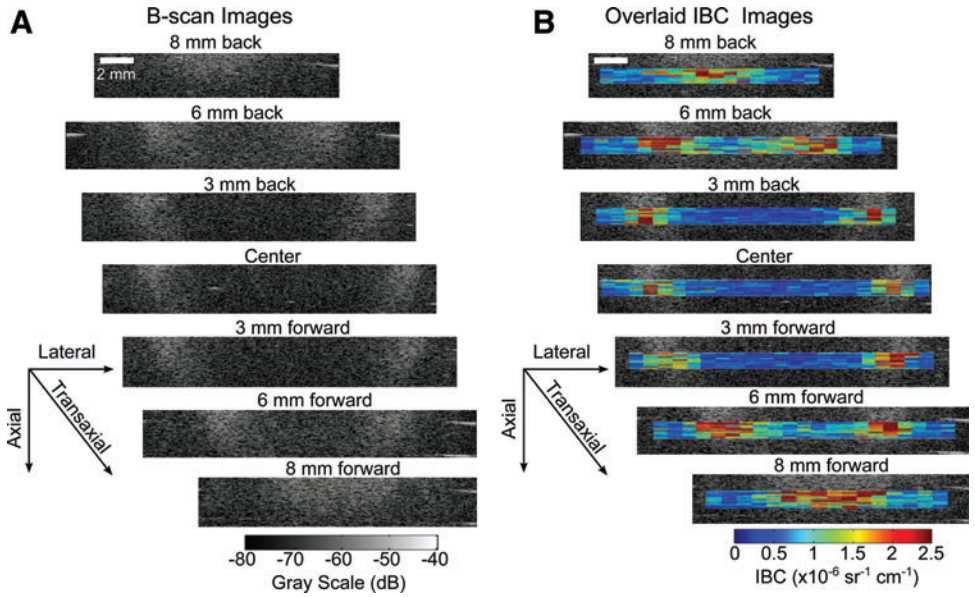

FIG. 7. Volumetric imaging of 3D collagen gels in tissue culture plates. Collagen hydrogels (2 mg/mL) were polymerized in 12-well tissue culture plates at 37°C for 1 h. The gels were 9 mm thick and 22 mm in diameter. Shown are representative **(A)** B-scan and **(B)** overlaid IBC parametric color images obtained beginning at one edge of the gel, with the transducer focused 4.5 mm below the surface of the gel. The IBC was estimated using the backscatter RF data of selected ROIs in B-scan images. Each color pixel represents an ROI with a lateral length of 850 μm (eight RF lines) and an axial length of 41 μm (one pulse length). Images shown represent one of 3 gels analyzed. Scale bar, 2 mm. Color images available online at www.liebertpub.com/tec

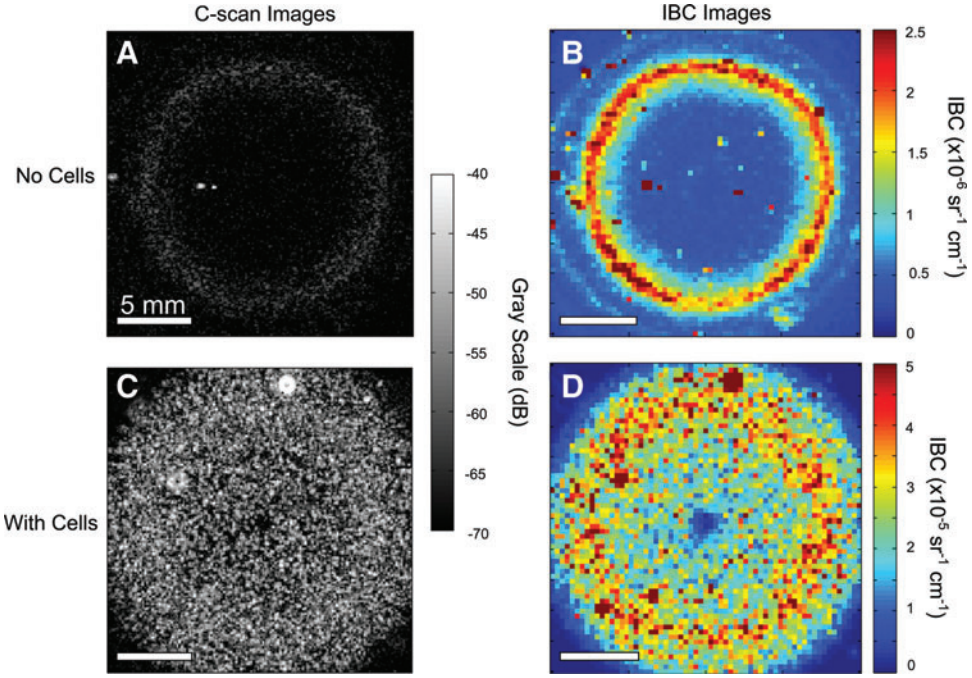

FIG. 8. C-scan and IBC parametric imaging of collagen gels. Collagen (2 mg/mL) gels were fabricated in 12-well tissue culture plates in the absence **(A, B)** and presence **(C, D)** of cells. Gels were polymerized for 1 h at 37°C. The gels were 9 mm thick and 22 mm in diameter. C-scan images of the **(A)** acellular and **(C)** cell-embedded gels are shown. The ultrasound transducer was focused at the middle of each gel (axial depth of 4.5 mm). Each pixel in the IBC images **(B, D)** corresponds to a 3D ROI with nine RF lines (three RF lines laterally, three RF lines transaxially) of 1-mm axial length. Images shown represent one of 3 gels analyzed. Scale bar, 5 mm. Note the colorbar scale in the IBC image of cell-embedded gels **(D)** is an order of magnitude greater than that of acellular gels **(B)**. Color images available online at www.liebertpub.com/tec

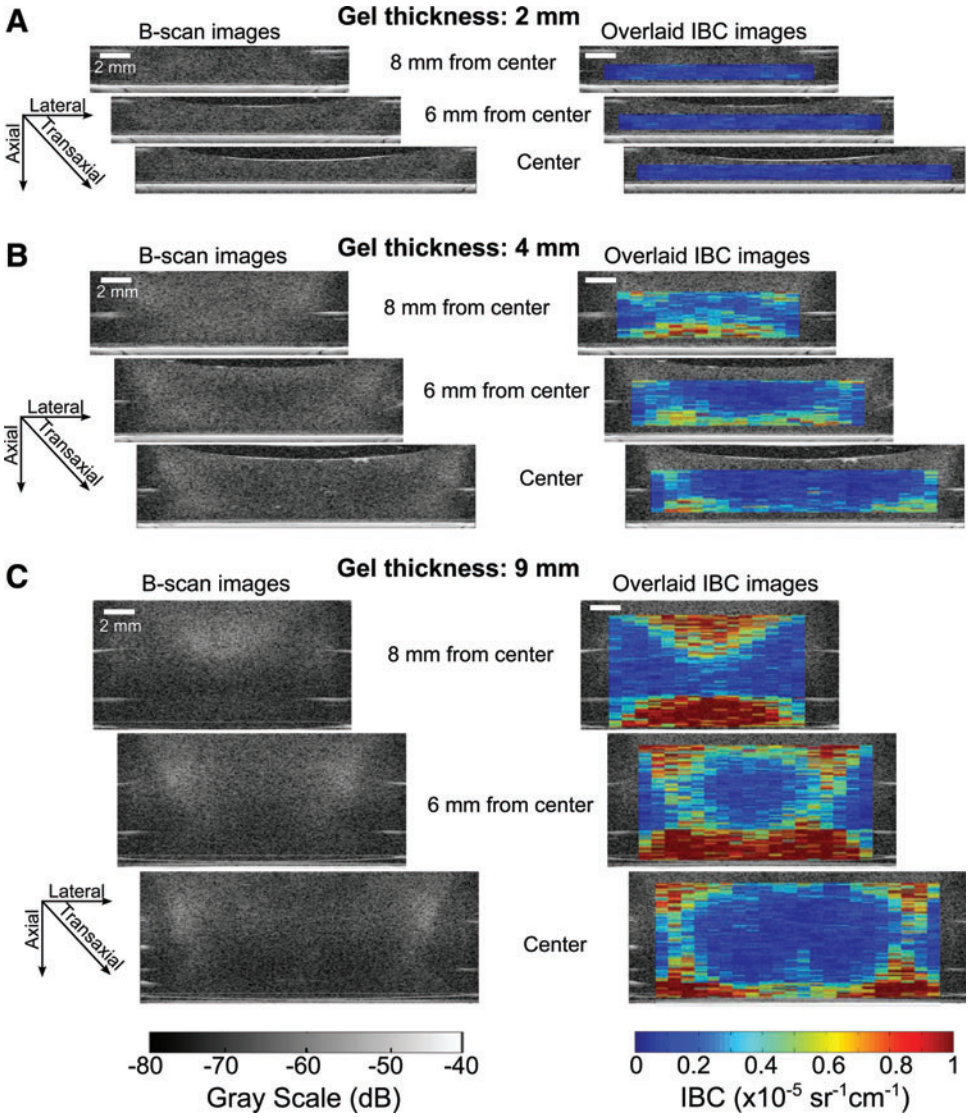

FIG. 9. Imaging of three-dimensional (3D) collagen gels of different thickness. Collagen hydrogels (2 mg/mL) were polymerized in 12-well tissue culture plates at 37°C for 1 h. The gels were 22 mm in diameter with thickness of either **(A)** 2, **(B)** 4, or **(C)** 9 mm. Shown are representative B-scan and overlaid IBC parametric images obtained at the gel center, and at 6 and 8 mm from the gel center. B-scan images shown are focused at the middle region of the gel at axial depths of 1, 2, and 4 mm within the 2, 4, and 9-mm thick gels, respectively. The IBC was estimated using the backscattered RF data collected at multiple depths, spanning the thickness of the gel. Each color pixel in the IBC images corresponds to a ROI with a lateral length of 850 μm (eight RF lines) and an axial length of 41 μm (one pulse length). Images shown represent one of at least 3 gels analyzed for each gel thickness. Scale bar, 2 mm. Color images available online at www.liebertpub.com/tec

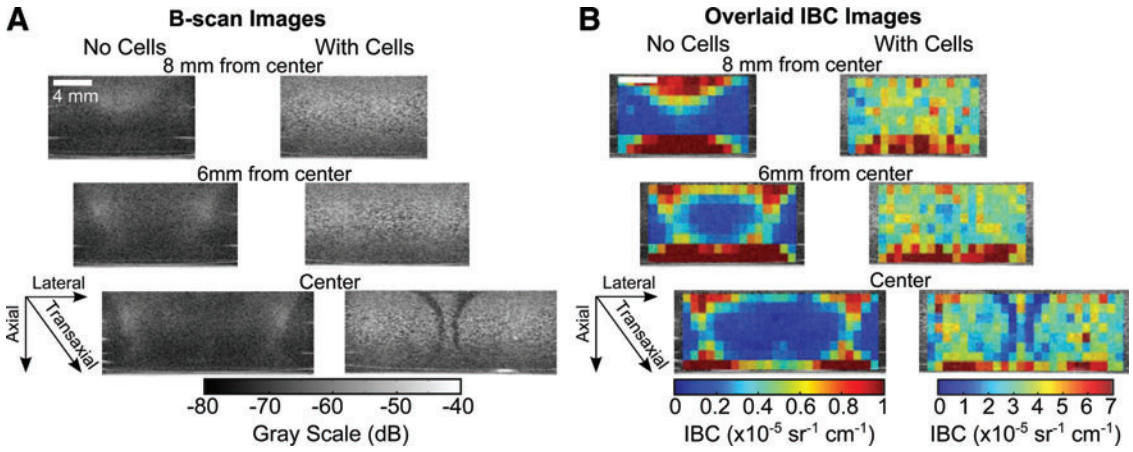

FIG. 10. B-scan and IBC imaging of acellular and cell-embedded gels. Collagen (2 mg/mL) gels were fabricated in 12-well tissue culture plates in the absence and presence of cells. The gels were 9 mm thick and 22 mm in diameter. Shown are representative **(A)** B-scan and **(B)** overlaid IBC parametric images obtained at the gel center, and at 6 and 8 mm from the gel center. The IBC was estimated using the backscattered RF data collected at multiple depths, spanning the thickness of the gel. Each pixel in the IBC images **(B)** corresponds to an ROI with eight RF lines (850 μm laterally) of 1-mm axial length (25 pulse lengths). Images shown represent one of at least three gels analyzed. Scale bar, 4 mm. Note the colorbar scale in the IBC images of the cell-embedded gel is an order of magnitude higher than that of the acellular gel. Color images available online at www.liebertpub.com/tec

Quantitative IBC imaging indicated cell densities in regions at the bottom and periphery of the gels were approximately sevenfold higher than that of the central core (Fig. 10B). Importantly, a comparison of IBC images of acellular and cell-embedded collagen gels indicated that cells accumulated at regions of increased collagen backscatter (Fig. 10B).

Discussion

Ultrasound provides a noninvasive and nondestructive approach for imaging tissues and biomaterials. Although conventional B-scan imaging is useful for rapid screening and imaging (e.g., Figs. 5 and 7A), the grayscale images are highly dependent on the transducer's characteristics and imaging system settings. Unlike B-scan imaging, quantitative ultrasound parameters are independent of the ultrasound system settings or transducer characteristics, and therefore these can provide quantitative metrics useful for assessment. In this study, we developed a high-frequency quantitative ultrasound technique based on the IBC to detect, quantify, and visualize regional differences in collagen fiber microstructure in 3D hydrogels noninvasively and nondestructively. A series of investigations demonstrated that the IBC increased linearly with increasing collagen concentration (Fig. 6A), and that the IBC decreased with increasing polymerization temperature (Fig. 6B). As confirmed with SHG imaging (Fig. 4), collagen fiber density increased with fabrication collagen concentration,[10] and collagen fiber diameter increased as polymerization temperature decreased.[2] Although the high-frequency source used in this study (38-MHz center frequency, 40-μm wavelength in water) does not have the resolution necessary to image individual collagen fibers, the IBC provides an estimate of the backscatter strength of sub-resolution scatterers per unit volume over the transducer bandwidth. Thus, the IBC provides a metric for quantifying variations in collagen backscatter produced by different collagen fiber density or diameter.

In contrast to SHG or SEM microscopy, the high-frequency IBC technique provides the capability for quantifying and visualizing collagen microstructure volumetrically throughout thick hydrogels. In this study, color-scaled parametric images of the IBC were generated with an axial resolution of 41 μm and lateral resolution of 850 μm. These IBC images provided quantitative visualization of collagen microstructure throughout entire volumes of the collagen hydrogels that were on the order of 1-cm thick (Figs. 7B, 8B, 9, and 10B). IBC parametric images were generated in either B-scan or C-scan imaging planes, or combined to provide volumetric imaging capabilities (Figs. 7–10). Regional variations in collagen microstructure were readily visualized using 3D quantitative IBC parametric images (Figs. 7B, 8B, 9, and 10B). For example, regional variations in collagen fiber microstructure were observed in collagen gels fabricated in standard tissue culture plates. These regional variations in collagen microstructure can arise from thermal gradients or low frequency vibrations often present in tissue culture incubators.[46] Thus, IBC imaging provides a valuable tool to evaluate collagen fiber microstructure noninvasively and volumetrically under common hydrogel fabrication conditions.

In this study, a comparison of IBC images of acellular and cell-embedded collagen gels indicated an organization of cells within areas of higher collagen IBC, suggesting that cells accumulated within regions of increased collagen fiber density or thickness (Figs. 8B and 10B). Our previous work demonstrated that the IBC technique can estimate cell concentration, and it has the potential to quantitatively monitor cell migration and proliferation in 3D engineered tissues.[25] The results of this study and those of our previous work[25] demonstrate how IBC parametric imaging can be used to investigate the relationship between collagen microstructure and cell behavior in 3D collagen gels.

For a given sample geometry and polymerization protocol, the IBC increased linearly with an increase in collagen concentration and decrease in polymerization temperature (Fig. 6). These differences in backscatter were consistent with the increases in collagen density and diameter observed with SHG imaging (Fig. 4). However, if fabrication conditions give rise to regional variations in collagen microstructure (e.g., thermal or ionic gradients and sample geometries), then the IBC alone cannot discern whether these regional variations are due to differences in collagen fiber density or diameter. To address this current limitation, techniques that combine more than one quantitative ultrasound parameter, such as the IBC and elastic modulus or acoustic attenuation, could be employed to distinguish between local variations in fiber density and diameter.

In summary, high-frequency ultrasound offers a noninvasive, nondestructive technology for quantitative imaging of collagen fiber microstructure in 3D hydrogels. The IBC is a system-independent metric for detecting and quantifying differences in collagen fiber microstructure. In addition, parametric IBC images provide volumetric, quantitative visualization of collagen microstructure throughout thick hydrogels. Thus, this IBC technique provides an important complement to current histology and microscopy techniques used to characterize collagen scaffolds. Further, the technique may be integrated into commercial ultrasound imaging devices for rapid, longitudinal assessment of 3D collagen-based engineered tissues.

Acknowledgments

The authors thank Sally Z. Child, MS, Eric Comeau, MS, Chris Farrar, MS, Emma Grygotis, and Jonathan Macoskey for technical assistance and helpful discussions. We gratefully acknowledge the support of the URMC Multiphoton Core Facility. This work was supported, in part, by grants R01EB008996 and R01EB018210 from the National Institutes of Health.

Disclosure Statement

No competing financial interests exist.

References

1. Miron-Mendoza, M., Seemann, J., and Grinnell, F. The differential regulation of cell motile activity through matrix stiffness and porosity in three dimensional collagen matrices. Biomaterials **31,** 6425, 2010.
2. Raub, C.B., Suresh, V., Krasieva, T., Lyubovitsky, J., Mih, J.D., Putnam, A.J., Tromberg, B.J., and George, S.C. Noninvasive assessment of collagen gel microstructure and mechanics using multiphoton microscopy. Biophys J **92,** 2212, 2007.

3. Yang, Y.L., Leone, L.M., and Kaufman, L.J. Elastic moduli of collagen gels can be predicted from two-dimensional confocal microscopy. Biophys J **97,** 2051, 2009.
4. Achilli, M., and Mantovani, D. Tailoring mechanical properties of collagen-based scaffolds for vascular tissue engineering: the effects of ph, temperature and ionic strength on gelation. Polymers Basel **2,** 664, 2010.
5. Sung, K.E., Su, G., Pehlke, C., Trier, S.M., Eliceiri, K.W., Keely, P.J., Friedl, A., and Beebe, D.J. Control of 3-dimensional collagen matrix polymerization for reproducible human mammary fibroblast cell culture in microfluidic devices. Biomaterials **30,** 4833, 2009.
6. Carey, S.P., Kraning-Rush, C.M., Williams, R.M., and Reinhart-King, C.A. Biophysical control of invasive tumor cell behavior by extracellular matrix microarchitecture. Biomaterials **33,** 4157, 2012.
7. Wolf, K., Alexander, S., Schacht, V., Coussens, L.M., von Andrian, U.H., van Rheenen, J., Deryugina, E., and Friedl, P. Collagen-based cell migration models *in vitro* and *in vivo*. Sem Cell Dev Biol **20,** 931, 2009.
8. Sander, E.A., and Barocas, V.H. Biomimetic collagen tissues: collagenous tissue engineering and other applications. In: Fratzl, P., ed. Collagen Structure and Mechanics. New York: Springer, 2008, p. 475.
9. Sevilla, C.A., Dalecki, D., and Hocking, D.C. Extracellular matrix fibronectin stimulates the self-assembly of microtissues on native collagen gels. Tissue Eng Part A **16,** 3805, 2010.
10. Roeder, B.A., Kokini, K., Sturgis, J.E., Robinson, J.P., and Voytik-Harbin, S.L. Tensile mechanical properties of three-dimensional type 1 collagen extracellular matrices with varied microstructure. J Biomech Eng **124,** 214, 2002.
11. Kreitz, S., Dohmen, G., Hasken, S., Schmitz-Rode, T., Mela, P., and Jockenhoevel, S. Nondestructive method to evaluate the collagen content of fibrin-based tissue engineered structures via ultrasound. Tissue Eng Part C Methods **17,** 1021, 2011.
12. Fite, B.Z., Decaris, M., Sun, Y., Sun, Y., Lam, A., Ho, C.K., Leach, J.K., and Marcu, L. Noninvasive multimodal evaluation of bioengineered cartilage constructs combining time-resolved fluorescence and ultrasound imaging. Tissue Eng Part C Methods **17,** 495, 2011.
13. Oe, K., Miwa, M., Nagamune, K., Sakai, Y., Lee, S.Y., Niikura, T., Iwakura, T., Hasegawa, T., Shibanuma, N., Hata, Y., Kuroda, R., and Kurosaka, M. Nondestructive evaluation of cell numbers in bone marrow stromal cell/beta-tricalcium phosphate composites using ultrasound. Tissue Eng Part C Methods **16,** 347, 2010.
14. Solorio, L., Babin, B.M., Patel, R.B., Mach, J., Azar, N., and Exner, A.A. Noninvasive characterization of *in situ* forming implants using diagnostic ultrasound. J Controlled Release **143,** 183, 2010.
15. Lizzi, F.L., Astor, M., Liu, T., Deng, C., Coleman, D., and Silverman, R. Ultrasonic spectrum analysis for tissue assays and therapy evaluation. Int J Imaging Syst Tech **8,** 3, 1997.
16. Gudur, M., Rao, R.R., Hsiao, Y.S., Peterson, A.W., Deng, C.X., and Stegemann, J.P. Noninvasive, quantitative, spatiotemporal characterization of mineralization in three-dimensional collagen hydrogels using high-resolution spectral ultrasound imaging. Tissue Eng Part C Methods **18,** 935, 2012.
17. Ghoshal, G., Oelze, M.L., and O'Brien, W.D. Quantitative ultrasound history and successes. In: Mamou, J., and Oelze, M.L., eds. Quantitative Ultrasound in Soft Tissues. New York: Springer, 2013, p. 21.
18. Taggart, L.R., Baddour, R.E., Giles, A., Czarnota, G.J., and Kolios, M.C. Ultrasonic characterization of whole cells and isolated nuclei. Ultrasound Med Biol **33,** 389, 2007.
19. Szabo, T.L. Diagnostic Ultrasound Imaging: Inside Out. Burlington, MA: Elsevier Academic Press, 2004.
20. Raju, B.I., Swindells, K.J., Gonzalez, S., and Srinivasan, M.A. Quantitative ultrasonic methods for characterization of skin lesions *in vivo*. Ultrasound Med Biol **29,** 825, 2003.
21. Zhang, D., Gong, X.F., and Ye, S.G. Acoustic nonlinearity parameter tomography for biological specimens via measurements of the second harmonics. J Acoust Soc Am **99,** 2397, 1996.
22. Waag, R.C., Lee, P.P.K., Lerner, R.M., Hunter, L.P., Gramiak, R., and Schenk, E.A. Angle scan and frequency-swept ultrasonic scattering characterization of tissue. In: White, D., and Lyons, E.A., eds. Ultrasound in Medicine. NY: Plenum Press, 1978, p. 563.
23. Insana, M.F., Wagner, R.F., Brown, D.G., and Hall, T.J. Describing small-scale structure in random media using pulse-echo ultrasound. J Acoust Soc Am **87,** 179, 1990.
24. Insana, M.F., and Hall, T.J. Parametric ultrasound imaging from backscatter coefficient measurements: image formation and interpretation. Ultrason Imaging **12,** 245, 1990.
25. Mercado, K.P., Helguera, M., Hocking, D.C., and Dalecki, D. Estimating cell concentration in three-dimensional engineered tissues using high frequency quantitative ultrasound. Ann Biomed Eng **42,** 1292, 2014.
26. Libgot-Calle, R., Ossant, F., Gruel, Y., Lermusiaux, P., and Patat, F. High frequency ultrasound device to investigate the acoustic properties of whole blood during coagulation. Ultrasound Med Biol **34,** 252, 2008.
27. Ghoshal, G., Kemmerer, J.P., Karunakaran, C., Abuhabsah, R., Miller, R.J., Sarwate, S., and Oelze, M.L. Quantitative ultrasound imaging for monitoring *in situ* high-intensity focused ultrasound exposure. Ultrason Imaging **36,** 239, 2014.
28. Lizzi, F.L., Astor, M., Feleppa, E.J., Shao, M., and Kalisz, A. Statistical framework for ultrasonic spectral parameter imaging. Ultrasound Med Biol **23,** 1371, 1997.
29. Kolios, M.C., Czarnota, G.J., Lee, M., Hunt, J.W., and Sherar, M.D. Ultrasonic spectral parameter characterization of apoptosis. Ultrasound Med Biol **28,** 589, 2002.
30. Lizzi, F., Ostromogilsky, M., Feleppa, E., Rorke, M., and Yaremko, M. Relationship of ultrasonic spectral parameters to features of tissue microstructure. IEEE Trans Ultrason Ferroelectr Freq Control **34,** 319, 1986.
31. Katouzian, A., Sathyanarayana, S., Baseri, B., Konofagou, E.E., and Carlier, S.G. Challenges in atherosclerotic plaque characterization with intravascular ultrasound (IVUS): from data collection to classification. IEEE Trans Inform Tech Biomed **12,** 315, 2008.
32. Brand, S., Weiss, E.C., Lemor, R.M., and Kolios, M.C. High frequency ultrasound tissue characterization and acoustic microscopy of intracellular changes. Ultrasound Med Biol **34,** 1396, 2008.
33. Raju, B.I., and Srinivasan, M.A. High-frequency ultrasonic attenuation and backscatter coefficients of *in vivo* normal human dermis and subcutaneous fat. Ultrasound Med Biol **27,** 1543, 2001.
34. Vlad, R.M., Brand, S., Giles, A., Kolios, M.C., and Czarnota, G.J. Quantitative ultrasound characterization of responses to radiotherapy in cancer mouse models. Clin Cancer Res **15,** 2067, 2009.
35. Kemmerer, J.P., and Oelze, M.L. Ultrasonic assessment of thermal therapy in rat liver. Ultrasound Med Biol **38,** 2130, 2012.

36. Dalecki, D., and Hocking, D.C. Ultrasound technologies for biomaterials fabrication and imaging. Ann Biomed Eng 2014 [Epub ahead of print] DOI: 10.1007/s10439-014-1158-6
37. Gudur, M.S., Rao, R.R., Peterson, A.W., Caldwell, D.J., Stegemann, J.P., and Deng, C.X. Noninvasive quantification of *in vitro* osteoblastic differentiation in 3d engineered tissue constructs using spectral ultrasound imaging. PLoS One **9,** e85749, 2014.
38. Kim, K., Jeong, C.G., and Hollister, S.J. Non-invasive monitoring of tissue scaffold degradation using ultrasound elasticity imaging. Acta Biomater **4,** 783, 2008.
39. Yu, J., Takanari, K., Hong, Y., Lee, K.W., Amoroso, N.J., Wang, Y.D., Wagner, W.R., and Kim, K. Non-invasive characterization of polyurethane-based tissue constructs in a rat abdominal repair model using high frequency ultrasound elasticity imaging. Biomaterials **34,** 2701, 2013.
40. Chen, X.C., Phillips, D., Schwarz, K.Q., Mottley, J.G., and Parker, K.J. The measurement of backscatter coefficient from a broadband pulse-echo system: a new formulation. IEEE Trans Ultrason Ferroelectr Freq Control **44,** 515, 1997.
41. Pinkerton, J.M.M. The absorption of ultrasonic waves in liquids and its relation to molecular constitution. Proc Phys Soc **62,** 129, 1949.
42. Bamber, J.C. Ultrasonic properties of tissues. In: Duck, F.A., Baker, A.C., and Starritt, H.C., eds. Ultrasound in Medicine. Bristol, UK: Institute of Physics Publishing, 1998, p. 57.
43. Oelze, M.L., and O'Brien, W.D., Jr. Defining optimal axial and lateral resolution for estimating scatterer properties from volumes using ultrasound backscatter. J Acoust Soc Am **115,** 3226, 2004.
44. Garvin, K.A., VanderBurgh, J., Hocking, D.C., and Dalecki, D. Controlling collagen fiber microstructure in three-dimensional hydrogels using ultrasound. J Acoust Soc Am **134,** 1491, 2013.
45. Guidance for Industry: Bioanalytical Method Validation. U.S. Department of Health and Human Services, Rockville, MD, 2001.
46. Davis, J.M. Basic techniques and media, the maintenance of cell lines, and safety. In: Davis, J.M., ed. Animal Cell Culture: Essential Methods. West Sussex, UK: John Wiley & Sons Ltd., 2011, p. 144.

Address correspondence to:
Diane Dalecki, PhD
Department of Biomedical Engineering
310 Georgen Hall, P.O. Box 270168
University of Rochester
Rochester, NY 14627

E-mail: dalecki@bme.rochester.edu

Received: September 4, 2014
Accepted: December 1, 2014
Online Publication Date: March 11, 2015